Biointerface Research in Applied Chemistry
Open-Access Journal (ISSN: 2069-5837)

Article
Volume 15, Issue 2, 2025, 28
https://doi.org/10.33263/BRIAC152.028

White Synthesis of $ZnO/TiO_2/g\text{-}C_3N_4$ Nanoparticles and their Photocatalytic Activity for Polyvinyl Chloride Microplastic Film Degradation

Jameel Mohammed Musthafa [1], Badal Kumar Mandal [1,*]

[1] Trace Elements Speciation Research Laboratory, Department of Chemistry, School of Advanced Sciences, Vellore Institute of Technology, Vellore - 632014, Tamil Nadu, India; mohammedmusthafa.j@vit.ac.in (J.M.M.); badalmandal@vit.ac.in (B.K.M.);
* Correspondence: badalmandal@vit.ac.in;

Scopus Author ID 7102080708

Received: 17.07.2024; Accepted: 5.05.2025; Published: 15.04.2025

Abstract: A novel photodegradable $ZnO/TiO_2/g\text{-}C_3N_4$ (zinc oxide/titanium dioxide/graphitic carbon nitride) nanoparticle (NP) was synthesized using the sol-gel method and sunlight-mediated degradation of polyvinyl chloride (PVC) microplastic (MP) films. The optical and structural properties of the sol-gel method were investigated using a variety of characterization methods, like Fourier transform infrared (FT-IR), UV-vis diffuse reflectance spectroscopy (UV-vis DRS), X-ray diffractometer (XRD) analysis, X-ray photoelectron spectroscopy (XPS), high-resolution transmission electron microscopy (HR-TEM), scanning electron microscopy (SEM) with energy dispersive X-ray (EDX) analysis, and thermogravimetric analysis (TGA). Degradation study results suggest that the photocatalytic activity of $ZnO/TiO_2/g\text{-}C_3N_4$/PVC nanocomposites (NCs) films was greater than that of pure PVC films, ZnO/PVC NCs films, TiO_2/PVC NCs films, $g\text{-}C_3N_4$/PVC NCs films, $ZnO/g\text{-}C_3N_4$/PVC NCs films, $TiO_2/g\text{-}C_3N_4$/PVC NCs films, and ZnO/TiO_2/PVC NCs films. Because of their increased optical absorption and efficient suppression of photo-produced charge carriers' recombination, the $ZnO/TiO_2/g\text{-}C_3N_4$/PVC NCs films showed higher photocatalytic degradation than various PVC films. Thus, PVC films with $ZnO/TiO_2/g\text{-}C_3N_4$ (5:5:2% wt) composite showed degradation of around 40% among pure PVC films, ZnO/PVC NCs films, TiO_2/PVC NCs films, $g\text{-}C_3N_4$/PVC NCs films, $ZnO/g\text{-}C_3N_4$/PVC NCs films, $TiO_2/g\text{-}C_3N_4$/PVC NCs films, and ZnO/TiO_2/PVC NCs films under visible sunlight over a short period of 30 days (240 h). The formation of carbonyl groups (-C=O) in the degradation product of PVC was confirmed by FT-IR analysis. When compared to the original PVC MPs, the $ZnO/TiO_2/g\text{-}C_3N_4$/PVC NCs films showed a significant decrease in crystallinity and carbonyl indexes, as much as 2.84% lower. The present research also suggests a photocatalytic mechanism, which may explain the increased photocatalytic activity.

Keywords: sol-gel method; $ZnO/TiO_2/g\text{-}C_3N_4$ NPs; PVC MPs; sunlight; photocatalytic degradation.

1. Introduction

PVC is a material that is widely used in both industry and daily life. Examples of its uses include building materials, packaging, and automobile components [1–3]. However, because of its non-biodegradability and chemical inertness, it is hard to degrade in garbage and in natural environments. One of the main causes of "white pollution" in the environment is PVC plastic [4]. Nowadays, the primary methods used to dispose of waste plastics include cracking catalysis, incineration, landfilling, and recycling [5]. Since degradable PVC-based plastics are almost completely non-recyclable and conventional treatment techniques cannot adequately address environmental pollution issues and may even exacerbate secondary pollution, they hold great promise as a potential solution to the expanding waste PVC plastic pollution problem. The reported degradation processes of PVC plastic include photodegradation, biodegradation, and thermo-oxidative degradation [6–8].

Among these, photodegradation might use solar energy, which is plentiful and sustainable and can lead to good energy consumption and cost-effectiveness. As a result, there is a great deal of interest in the photodegradation process [9,10]. Plastics can break down into smaller molecules by breaking their chemical bonds, which can turn into useful products or completely mineralize into CO_2 and H_2O [11]. Plastics eventually break down into organic compounds due to irregular polymer chain breakage, which can happen in any monomer in the polymer. Certain polymers have a chain fracture at the end of the monomer repeating unit, which causes the remaining monomers to break sequentially through chain depolymerization [12]. The products formed and the degradation methods differ depending on the kind of polymer and the surrounding environmental variables. Based on published research on the degradation of various plastics by AOPs (photodegradation processes, direct photocatalytic oxidation processes, and electrochemical oxidation processes), sulfate radical-AOPs have demonstrated superior catalytic degradation capability for the decomposition of cosmetic plastics primarily composed of polyethylene [13]. Plastics' high redox potentials could help in the oxidation process [14]. Furthermore, AOP-induced plastic degradation causes chain breakage, the production of valuable compounds, and even the entire mineralization of plastics.

Pure TiO_2-based photocatalysts lack efficient visible light photoactivity due to their quick charge carrier recombination rate and very large bandgap (3.2 eV). In the way of addressing the challenges with pure TiO_2, studies have evolved to improve electron-hole separation and visible light absorption through various methods such as anions or cations doping, developing NCs with sensitizing, and different metal oxides using plasmonic metals [15–17]. TiO_2 was combined with various metal oxides (e.g., Ag_2O, BiO_4, CeO_2, CuO, Fe_2O_3, WO_3, ZnO, and ZrO_2) [18], and improved photocatalytic activity was observed. Specifically, it has been shown that heterojunction formation between the other low-bandgap metal oxides and host semiconductors with different band edge positions is an effective way to increase photoactivity when exposed to visible light [19,20]. Several studies have demonstrated that local charge separation at the photocatalyst surface can be enhanced by crystal facets, co-catalyst doping, or local doping. [21,22]. Various bifunctional co-catalysts have also been proposed to improve charge separation [23]. ZnO and TiO_2 have band gaps of about 3.2 eV each [24]. However, because of its great quantum efficiency, ZnO outperformed TiO_2 in degrading organic pollutants [25]. Despite this, ZnO has been shown to photo-corrode in acidic aqueous solutions [26,27]. Because of their band energies, both ZnO and TiO_2 have effective photocatalytic activity when exposed to UV radiation but not when exposed to visible light [28]. The photocatalytic activities and visible light absorption capabilities of the TiO_2/ZnO composite were found to be higher in comparison to ZnO or TiO_2 [29]. The photodegradation of an organic dye by visible light was demonstrated to be efficient for the TiO_2/ZnO composite, and the reason for this was ascribed to charge transfer at the TiO_2/ZnO interface [30]. A study revealed the photocatalytic elimination of H_2S and xylene from TiO_2/ZnO composites. Recently, a TiO_2/ZnO composite calcined at 558°C with 2.1 wt% ZnO [31] showed better efficiency for the photodecomposition of nitrogen oxides (NO_x) under UV light.

g-C_3N_4 photocatalysts have an appropriate band gap (~ 2.7 eV), easy manufacture, cheap cost, and outstanding physical and chemical stability; they are now receiving a lot of interest. g-C_3N_4 as a useful photocatalyst for PVC photodegradation and to create a g-C_3N_4 photocatalyst with an appropriate structure and photoelectrochemical processes for enhanced PVC photocatalytic degradation abilities. It was discovered that incorporating g-C_3N_4 into PVC not only increased its mechanical qualities but also significantly enhanced its photodegradation under simulated sunlight [32]. Xiao-jing *et al*. reported that while the PVC-TiO_2 film lost just 1.4% of its weight under identical testing conditions, the weight of the plasma-treated PVC-TiO_2 film with irradiation rapidly fell, showing a 2.0% overall reduction in 60 hours [33]. Anirban Roy *et al*. [34] reported comparing the performances of NPs synthesized in various settings. After three hours, the maximum degradation of around 12% was achieved using NPs that were synthesized from power and temperature at 42 W and 30°C. According to Devika Sil *et al*. [35], after 90 minutes of solar radiation, artificial UV radiation could break down the PVC-ZnO composite into 6.2% of its initial weight, whereas decomposition from sun radiation was 14.2%.

Inspired by the above consideration, our objective of this study was i) to synthesize ZnO/TiO_2/g-C_3N_4 NPs using the sol-gel synthesis technique; ii) to characterize ZnO/TiO_2/g-C_3N_4 NPs by different instrumental techniques such as UV-Vis, XRD, HR-TEM-EDAX, SEM-EDAX, FT-IR, and XPS; iii) to prepare ZnO/TiO_2/g-C_3N_4/PVC NCs film; iv) to assess degradation products by FT-IR analyses; and v) finally to propose a plausible photodegradation mechanism of PVC composite film by ZnO/TiO_2/g-C_3N_4 NPs.

2. Materials and Methods

2.1. Reagents.

Zinc acetate ($C_4H_6O_4Zn$ x $2H_2O$), titanium dioxide (TiO_2), melamine (g-C_3N_4), nitric acid (HNO_3), sodium hydroxide, dimethylformamide (DMF), double distilled water (DDW), and PVC MPs particles (radius 2 mm) were bought from Sigma-Aldrich in Tamil Nadu, India, and the remaining other chemicals were of analytical quality.

2.2.1. Preparation of ZnO/TiO_2 NPs.

Initially, TiO_2 NPs were synthesized using the sol-gel method, followed by ZnO NPs, which were synthesized and doped with TiO_2 NPs, given the designation ZnO-doped TiO_2 (ZnO/TiO_2) NPs. The synthesis of (ZnO/TiO_2) NPs was carried out as follows:

2.2.2. Synthesis of TiO_2 NPs via the sol-gel method.

The precursor solution was initially prepared by adding 2 g of TiO_2 to 20 mL of 100% ethanol with vigorous magnetic stirring for 30 minutes. Then, under constant stirring, 5 mL of 100% ethanol (C_2H_5OH), 3 mL of DDW, and 0.5 mL of HNO_3 acid were added dropwise to the solution, bringing the pH to around 2. The achieved translucent yellow sol was aged for 8 hours while being stirred continuously for 5 hours at room temperature to create a white, homogeneous gel. This gel was dried at 80°C to dry it out and turn it into nanocrystalline TiO_2. The produced TiO_2 nanopowders were employed to create NPs after being calcined at 400°C for two hours in a muffle furnace using finely ground crystals. This synthesis process was done using a variety of references to give the TiO_2 NPs [36–38].

2.2.3. Synthesis of ZnO-doped TiO_2 (ZnO/TiO_2) NPs.

ZnO/TiO_2 NPs were synthesized using the ultrasound-assisted sol-gel technique and modifying the Prasannalakshmi *et al*. process [39]. This study's procedure for preparing a homogenous ZnO solution was as follows: By magnetic stirring, 2 g of zinc acetate was introduced to 40 mL of DDW and thoroughly dissolved therein. The aforementioned solution was then dropped into the added 40 mL of prepared 0.5M sodium hydroxide (NaOH) solution while being stirred magnetically at a higher speed. Following that, 750 mg of TiO_2 NPs that had already been synthesized were added to this ZnO solution while it was sonicated for 30 minutes. To create a gel, the entire liquid was continually agitated for 4 hours. The resultant gel underwent multiple washings before being dried at 90°C. After being annealed at 550°C for 4 hours, this ZnO/TiO_2 sample with a 1:1 molar ratio was finally given the designation ZnO/TiO_2. The identical technique was followed exactly, with the exception that the amount of TiO_2 used to create ZnO/TiO_2 was 1.5 g rather than the desired 1:1 molar ratio. For eventual usage, these NPs were synthesized many times.

2.2.4. Synthesis of g-C_3N_4.

A 3 g sample of melamine was heated in a muffle furnace for 4 hours at a temperature of 50°C per minute to 550°C in the air within a crucible made of alumina with a lid. The acquired material was processed into a yellow powder in a mortar and was named g-C_3N_4 [40].

2.2.5. Synthesis of ZnO/TiO_2/g-C_3N_4 NPs.

Using the same process but a different amount of TiO_2 (1.5 g), ZnO/TiO_2/g-C_3N_4 preparation was made, resulting in ZnO/TiO_2/g-C_3N_4 NPs with a molar ratio of 5:5:2% wt, as shown in Figure 1.

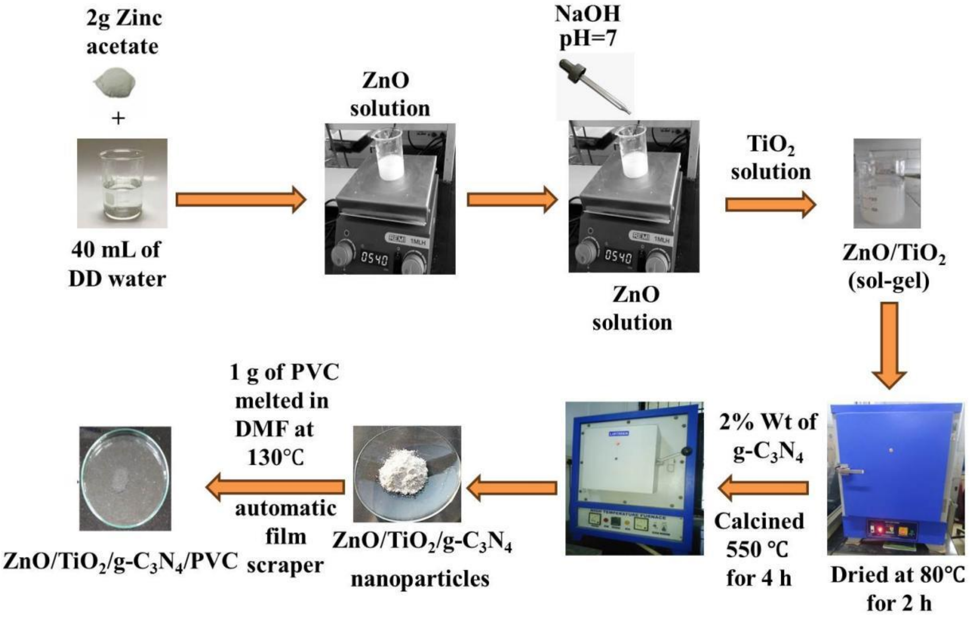

Figure 1. Diagram illustrating the sol-gel method's preparation of ZnO/TiO_2/g-C_3N_4/PVC (NCs) film.

2.2.6. Preparation and photocatalytic degradation of ZnO/TiO_2/g-C_3N_4/PVC NCs films.

Initiating the ZnO/TiO_2/g-C_3N_4 NPs and PVC film involved adding approximately 1 g of PVC film to 80 ml of DMF and aggressively stirring. After PVC is completely melted in the

DMF solvent at 130°C, 5% wt of ZnO/TiO_2 and 2% wt of g-C_3N_4 photocatalysts are added and evenly distributed while stirring and vacuum-drying [41]. The mixture was then ultrasonically processed for 10 minutes. After being dried for 2 hours at 80°C in a hot air oven and later in a water bath at 30°C for 48 hours. After equally distributing the mixture on the film-forming plate of the automatic film scraper, room temperature and atmospheric pressure were used to create a 150-µm film. The ZnO/TiO_2/g-C_3N_4/PVC NCs film was developed by removing the film-forming plate and immersing it in DDW to allow a natural film to form [42].

For a duration of 30 days (240 hours), the degradation of ZnO/TiO_2/g-C_3N_4/PVC NCs film under solar light was carried out on a petri dish in the open air under atmospheric conditions every sunny day from 9:00 a.m. to 5:00 p.m. For the same period of time, a different sample of ZnO/TiO_2/g-C_3N_4/PVC NCs film was kept in the dark.

2.3. Characterization of ZnO/TiO_2/g-C_3N_4/PVC NC films.

2.3.1. UV-visible (UV-Vis) spectroscopic analysis.

ZnO/TiO_2/g-C_3N_4 NPs were first characterized by UV-visible DRS spectroscopy (Jasco V-670 UV-vis DRS spectrophotometer). A UV-Vis DRS spectrum was obtained between 200 and 800 nm from the λmax.

2.3.2. Fourier transform infrared (FT-IR) analysis.

By utilizing FT-IR tests to determine the intensity of carbonyl groups, the degree of oxidation was observed. Using the JASCO FT-IR 4100 (Shimadzu IR AFFINITY-1) to capture the FT-IR spectra of these materials, the presence of functional groups in ZnO/TiO_2/g-C_3N_4/PVC was determined. Using KBr pellets, it was in the diffuse reflectance mode with a resolution of 4 cm^{-1}.

2.3.3. Scanning electron microscopy (SEM) with energy dispersive X-ray (EDX) analysis.

After dropping the aqueous dispersion of the solid NPs onto the Cu grid, they were dried in a vacuum oven in preparation for SEM-EDAX analysis. Additionally, ZnO/TiO_2/g-C_3N_4 NPs' chemical composition was examined using EDAX research (ZEISS EVO-MA 10, Oberkochen, Germany).

2.3.4. High-resolution transmission electron microscopy (HR-TEM) analysis.

Techni G20Twin, FEI high-resolution transmission electron microscopy (HR-TEM) was used at 200 kV. A drop of synthesized ZnO/TiO_2/g-C_3N_4 NPs was placed on a copper grid coated with carbon to prepare the sample, and it was dried for 120 minutes at 24 ± 2°C. The specimen holder held the sample in place. The 1.8.0 version of Image J software was used to calculate the particle size of ZnO/TiO_2/g-C_3N_4 NPs. The HR-TEM was combined with selected area electron diffraction to study the NPs' crystalline structure.

2.3.5. X-ray photoelectron spectroscopy (XPS) analysis.

The data obtained from XPS (X-ray photoelectron spectroscopy) was gathered using a Thermo Scientific Escalab 250Xi spectrometer. ZnO/TiO_2/g-C_3N_4 chemical and electronic states, as well as elemental composition, can all be measured by XPS in a given material.

2.3.6. X-ray diffraction (XRD) analysis.

XRD studies were performed on the dried ZnO/TiO_2/g-C_3N_4 NPs using a Bruker D8 diffractometer equipped with Cukα radiation (λ = 1.54 nm). The analysis of the powder XRD was carried out within the scanning range (2θ value) of 10° to 90°. The step size was 0.02°, and the scanning rate was 4°/min.

2.3.7. Thermogravimetric (TGA) analysis.

The thermogravimetric (TGA) analysis of the weight loss experiment was conducted to investigate the degree of PVC MP film degradation in the presence of ZnO/TiO_2/g-C_3N_4/PVC NCs.

3. Results and Discussion

The ZnO/TiO_2/g-C_3N_4 NPs were blended with PVC to make composite films, which were then tested for their degradation by sunlight irradiation. UV-vis spectroscopy, XRD, XPS, FT-IR, and SEM-EDAX analysis were used to confirm preliminary ZnO/TiO_2/g-C_3N_4 NPs in the polymer matrix. The formation of carbonyl groups (-C=O) in the degradation product of PVC was confirmed by FT-IR analysis. The weight loss experiment was investigated by thermogravimetric (TGA) analysis to study the degree of degradation of polymer film in the presence of ZnO/TiO_2/g-C_3N_4 NPs. The photocatalytic degradation of PVC films in the presence of ZnO/TiO_2/g-C_3N_4 is finally explained by a hypothesized mechanism.

3.1. UV-vis DRS.

UV-vis DRS was used to analyze the optical characteristics at room temperature. The UV-visible spectrum, which ranges from 200 nm to 800 nm, displays the absorption spectra (Figure 2). In Figure 2a, the adsorption edges of ZnO NPs, TiO_2 NPs, g-C_3N_4 NPs, ZnO/g-C_3N_4 NPs, TiO_2/g-C_3N_4 NPs, ZnO/TiO_2 NPs, and ZnO/TiO_2/g-C_3N_4 NPs are 300–450 nm [32, 43–46], respectively, proving that UV light is the only source of excitement for them.

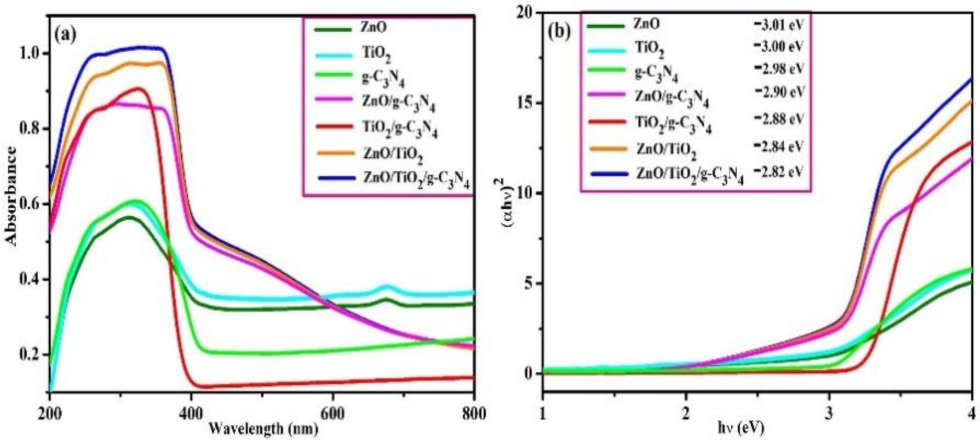

Figure 2. (a) UV-visible DRS spectrum of ZnO NPs, TiO_2 NPs, g-C_3N_4 NPs, ZnO/g-C_3N_4 NPs, TiO_2/g-C_3N_4 NPs, ZnO/TiO_2 NPs, and ZnO/TiO_2/g-C_3N_4 NPs; **(b)** the band gap of the as-obtained ZnO NPs, TiO_2 NPs, g-C_3N_4 NPs, ZnO/g-C_3N_4 NPs, TiO_2/g-C_3N_4 NPs, ZnO/TiO_2 NPs, and ZnO/TiO_2/g-C_3N_4 NPs.

ZnO/TiO_2/g-C_3N_4 NPs, on the other hand, exhibit high absorption in the visible region. Although the light absorption intensity of ZnO NPs, TiO_2 NPs, g-C_3N_4 NPs, ZnO/g-C_3N_4 NPs, TiO_2/g-C_3N_4 NPs, and ZnO/TiO_2 NPs is lower than that of ZnO/TiO_2/g-C_3N_4 NPs, its UV-vis DRS sensitivity is still comparatively powerful.

Conversely, Figure 2b shows how Tauc's equation is used to predict the bandgap energy values of ZnO NPs, TiO_2 NPs, g-C_3N_4 NPs, ZnO/g-C_3N_4 NPs, TiO_2/g-C_3N_4 NPs, ZnO/TiO_2 NPs, and ZnO/TiO_2/g-C_3N_4 NPs [32, 43–46]. The band gap energy values of ZnO NPs, TiO_2 NPs, g-C_3N_4 NPs, ZnO/g-C_3N_4 NPs, TiO_2/g-C_3N_4 NPs, ZnO/TiO_2 NPs, and ZnO/TiO_2/g-C_3N_4 NPs are estimated at 3.01 eV, 3.00 eV, 2.98 eV, 2.90 eV, 2.88 eV, 2.84 eV, and 2.82 eV, respectively.

3.2. FT-IR analysis.

The FT-IR spectrum obtained for the ZnO NPs, TiO_2 NPs, g-C_3N_4 NPs, ZnO/g-C_3N_4 NPs, TiO_2/g-C_3N_4 NPs, ZnO/TiO_2 NPs, and ZnO/TiO_2/g-C_3N_4 NPs is shown in Figure 3. A wideband is displayed in the 3550–3200 cm^{-1} range, which corresponds to vibrations brought on by OH bond stretching. For g-C_3N_4, the absorption peaks at 1650–1200 and 805 cm^{-1} correlated with the triazine structure's out-of-plane bending vibration mode and the stretching vibration mode of the C=N bond and the C-N bond in aromatic heterocycles [47]. TiO_2's characteristic bands can be found between 900 and 700 cm^{-1} [48–50]. The Zn-O NPs stretching vibrations have been found in the 600–400 cm^{-1} range [51].

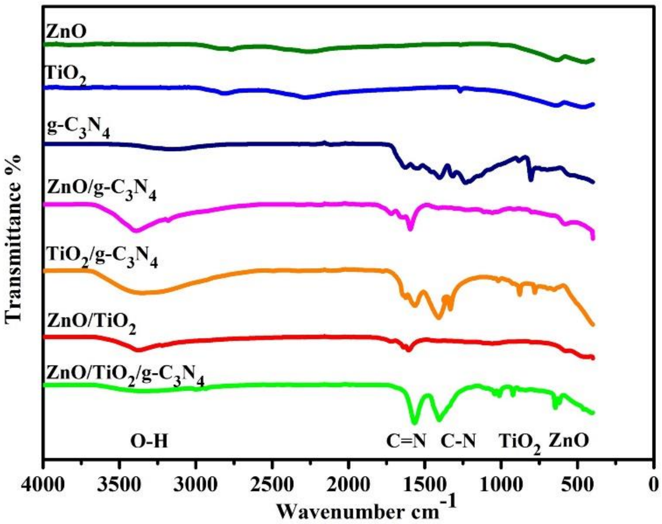

Figure 3. FT-IR spectrum of ZnO NPs, TiO_2 NPs, g-C_3N_4 NPs, ZnO/g-C_3N_4 NPs, TiO_2/g-C_3N_4 NPs, ZnO/TiO_2 NPs, and ZnO/TiO_2/g-C_3N_4 NPs.

3.3 HR-TEM and SEM-EDX analysis.

Figure 4a shows the surface morphology of ZnO NPs as observed by HR-TEM images. The ZnO NPs have a rough surface and exhibit a regular spherical morphology. The presence of Zn and O elements in the SEM-EDS image proves that the synthesized materials are ZnO NPs (Figure 4b). The SEM-EDS analysis shows clear peaks of Zn (70.53%) and O (29.47%) in the spectrum. Figure 4c shows the surface morphology of TiO_2 NPs as observed by HR-TEM images. The presence of Ti and O elements in the SEM-EDS image further proves that the synthesized materials are TiO_2 NPs (Figure 4d). The SEM-EDS analysis shows clear peaks of Ti (66.58%) and O (33.42%) in the spectrum. Figure 4e shows the surface morphology of g-C_3N_4 NPs as observed by HR-TEM images. The presence of C and N elements in the HR-TEM-EDS image proves that the synthesized materials are g-C_3N_4 NPs (Figure 4f). The HR-TEM-EDS analysis shows clear peaks of C (89.24%) and N (10.76%) in the spectrum.

Figure 4g shows the surface morphology of ZnO/g-C_3N_4 NPs as observed by HR-TEM images. The presence of O, C, N, and Zn elements in the SEM-EDS image proves that the synthesized materials are $ZnO/g\text{-}C_3N_4$ NPs (Figure 4h). The SEM-EDS analysis shows clear peaks of C (49.72%), N (21.47%), O (14.46%), and Zn (14.35%) in the spectrum. Figure 4i shows the surface morphology of $TiO_2/g\text{-}C_3N_4$ NPs as observed by HR-TEM images. The presence of O, C, N, and Ti elements in the SEM-EDS image proves that the synthesized materials are $TiO_2/g\text{-}C_3N_4$ (Figure 4j). The SEM-EDS analysis shows clear peaks of C (52.44%), N (10.51%), O (26.48%), and Ti (10.58%) in the spectrum. Figure 4k shows the surface morphology of ZnO/TiO_2 NPs as observed by HR-TEM images. The presence of O, Ti, and Zn elements in the SEM-EDS image proves that the synthesized materials are ZnO/TiO_2 NPs (Figure 4l). The EDS analysis shows clear peaks of O (47.44%), Ti (46.77%), and Zn (5.79%) in the spectrum. Figure 4m shows the surface morphology of $ZnO/TiO_2/g\text{-}C_3N_4$ NPs as observed by HR-TEM images. The presence of C, N, O, Ti, and Zn elements in the SEM-EDS image proves that the synthesized materials are $ZnO/TiO_2/g\text{-}C_3N_4$ NPs (Figure 4n). The SEM-EDS analysis shows clear peaks of C (50.29%), N (0.85%), O (30.61%), Ti (14.50), and Zn (3.75%) in the spectrum.

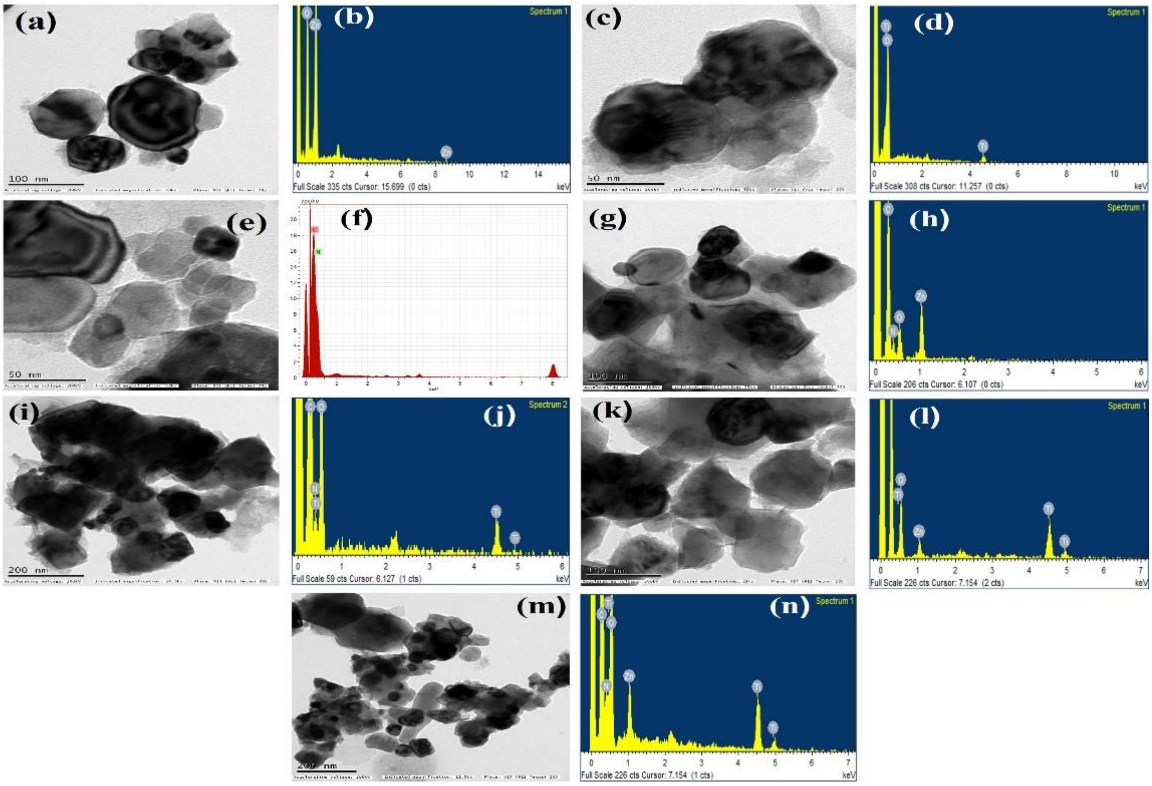

Figure 4. (a) HR-TEM image of ZnO NPs; **(b)** SEM-EDS spectrum of ZnO NPs; **(c)** HR-TEM image of TiO_2 NPs; **(d)** SEM-EDS spectrum of TiO_2 NPs; **(e)** HR-TEM image of $g\text{-}C_3N_4$ NPs; **(f)** HR-TEM-EDS spectrum of $g\text{-}C_3N_4$ NPs; **(g)** HR-TEM image of $ZnO/g\text{-}C_3N_4$ NPs; **(h)** SEM-EDS spectrum of $ZnO/g\text{-}C_3N_4$ NPs; **(i)** HR-TEM image of $TiO_2/g\text{-}C_3N_4$ NPs; **(j)** SEM-EDS spectrum of $TiO_2/g\text{-}C_3N_4$ NPs; **(k)** HR-TEM image of ZnO/TiO_2 NPs; **(l)** SEM-EDS spectrum of ZnO/TiO_2 NPs; **(m)** HR-TEM image of $ZnO/TiO_2/g\text{-}C_3N_4$ NPs; **(n)** SEM-EDS spectrum of $ZnO/TiO_2/g\text{-}C_3N_4$ NPs.

3.4. X-ray photoelectron spectroscopic analysis.

The $ZnO/TiO_2/g\text{-}C_3N_4$ NPs' XPS survey spectrum is shown in Figure 5a. The survey spectra were measured in the electron-binding energy range of 0 eV to 1200 eV. There was a 0.5 eV energy step and a 0.5 s dwell period. In the broad spectrum, photoelectrons (C1s, O1s, N1s, Ti2p, and Zn2p) were identified. The binding energies of the electrons in Zn2p, Ti2p, O1s, C1s, and N1s are shown in Figures 5 (b, c, d, e, and f). Two sets of $Zn2p_{3/2}$, $Zn2p_{1/2}$, and their satellite peaks were visible for the Zn2p peaks at energies of 1021.16 and 1044.26 eV, respectively. These energies correspond to Zn^{2+} in the $ZnO/TiO_2/g-C_3N_4$ NP in Figure 5(b) [52]. The $Ti2p_{3/2}$ and $Ti2p_{1/2}$ peaks may be distinguished from the Ti2p peak, respectively, at energies of 458.60 eV and 464.75 eV. This is consistent with the Ti^{4+} state in Figure 5(c) [53]. The 529.35 eV peak may be distinguished from the O1s peak in Figure 5(d) [54], respectively. It is possible to identify the 284.35 eV and 288.22 eV peaks in Figure 5(e) from the C1s peaks attributed to C-C and N-C=N [40], respectively. The 398.28 eV peak assigned to C-N=C may be distinguished from the N1s peak in Figure 5(f) [55], respectively.

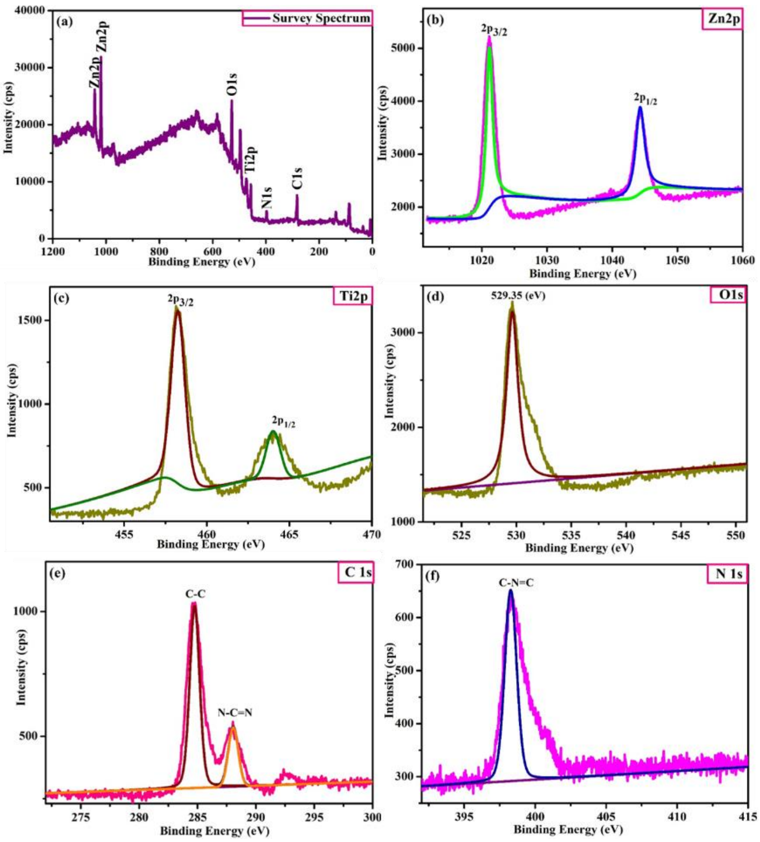

Figure 5. XPS survey spectrum of the **(a)** $ZnO/TiO_2/g-C_3N_4$ NPs; **(b)** Zn2p; **(c)** Ti2p; **(d)** O1s; **(e)** C1s; **(f)** N1s.

3.5. X-ray diffraction (XRD) analysis.

In Figure 6a, the ZnO phases (100), (002), (101), (102), (110), (103), and (112) were found to have the most prominent XRD peaks. 2θ values at 31°, 34°, 36°, 47°, 56°, 62°, and 67°, respectively, the ZnO peaks were measured. The reflections from ZnO's hexagonal wurtzite phase, designated by JCPDS number 00-036-1451, are represented by these peaks [56]. TiO_2 reflections (101), (103), (004), (220), (105), (211), and (204) are allocated to the peaks at 2θ values of 25.76°, 37.70°, 38.60°, 48.12°, 55.16°, 56.32°, and 64.21°. These values match JCPDS file No.00-075-1537, which validates the presence of the anatase phase in Figure 6b. According to the Scherrer equation [57], anatase TiO_2 has an average crystallite size of approximately 16.95 nm. The two XRD peaks that the pristine $g-C_3N_4$ displayed in Figure 6c were at 12.92° and 27.95°, respectively. These were attributed to the stacking of the conjugated aromatic structure and the in-plane repeating units of the continuous heptazine framework, which correspond to the (100) and (002) crystal planes [40]. For $ZnO/g-C_3N_4$, peaks at 2θ values of 12.35°, 27.52°, 31.80°, 34.62°, 36.18°, 47.75°, 56.81°, and 62.89° are reflections for $ZnO/g-C_3N_4$, which confirms the presence of hexagonal wurtzite phase in Figure 6d. For $TiO_2/g-C_3N_4$, peaks at 2θ values of 12.65°, 25.72°, 27.13°, 37.80°, 38.70°, 48.42°, 55.36°, 56.42°, and 64.31° are reflections for $TiO_2/g\text{-}C_3N_4$, which confirms the presence of hexagonal wurtzite phase in Figure 6e. ZnO/TiO_2 peaks at 2θ values of 25.57°, 31.99°, 34.67°, 36.52°, 38.03°, 47.80°, 48.29°, 55.30°, 56.86°, and 62.94° are reflections for ZnO/TiO_2 [58], which confirms the presence of the hexagonal wurtzite phase in Figure 6f. For $ZnO/TiO_2/g\text{-}C_3N_4$, peaks at 2θ values of 12.45°, 25.62°, 27.13°, 31.90°, 34.72°, 36.22°, 38.08°, 47.85°, 48.34°, 55.40°, 56.91°, and 62.99° are reflections for $ZnO/TiO_2/g\text{-}C_3N_4$, which confirms the presence of hexagonal wurtzite phase in Figure 6g.

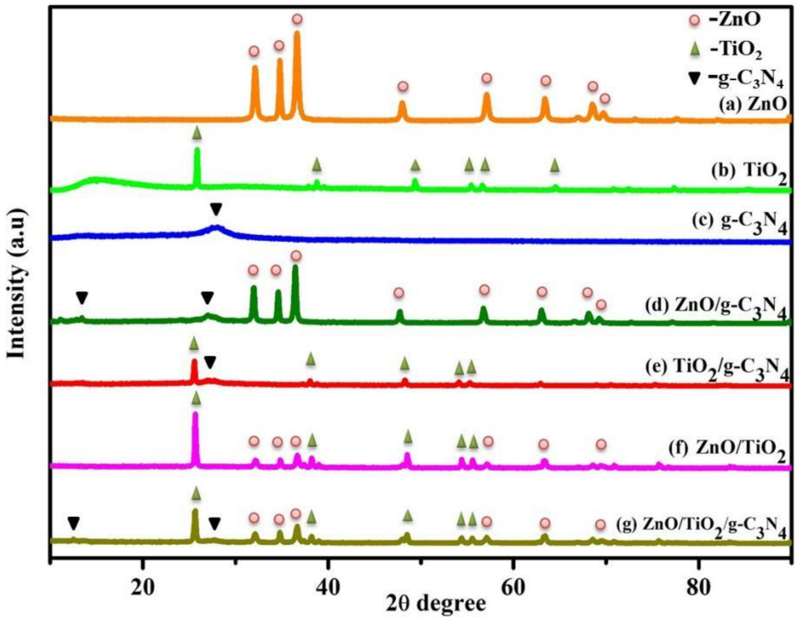

Figure 6. XRD pattern of **(a)** ZnO NPs; **(b)** TiO_2 NPs; **(c)** $g\text{-}C_3N_4$ NPs; **(d)** $ZnO/g\text{-}C_3N_4$ NPs; **(e)** $TiO_2/g\text{-}C_3N_4$ NPs; **(f)** ZnO/TiO_2 NPs; **(g)** $ZnO/TiO_2/g\text{-}C_3N_4$ NPs.

3.6. Photocatalytic application.

Photoinduced weight loss, thermogravimetric, SEM, and FT-IR analyses were used to monitor the light sensitivity of synthesized $ZnO/TiO_2/g\text{-}C_3N_4$ NPs for catalytic photodegradation of ZnO/PVC NCs films, TiO_2/PVC NCs films, $g\text{-}C_3N_4$/PVC NCs films, $ZnO/g\text{-}C_3N_4$/PVC NCs films, $TiO_2/g\text{-}C_3N_4$/PVC NCs films, ZnO/TiO_2/PVC NCs films, and $ZnO/TiO_2/g\text{-}C_3N_4$/PVC NCs films. Figure 7 shows the weight loss curves of various PVC NC films exposed to sunlight naturally. The results suggest higher weight loss of the $ZnO/TiO_2/g\text{-}C_3N_4$/PVC NCs film compared to that of various PVC films, and the weight reduction of the $ZnO/TiO_2/g\text{-}C_3N_4$/PVC NCs film was increased by irradiation time. Interestingly, we also found a weight reduction of 5.78 ± 0.10% of $ZnO/TiO_2/g\text{-}C_3N_4$/PVC NCs film in the dark after 240 h (Figure 7a). The maximum value of 39.86 ± 0.26 % weight loss was for $ZnO/TiO_2/g\text{-}C_3N_4$/PVC NCs film after 240 h of sunlight exposure (Figure 7b), compared to the weight reduction of various PVC films under a similar set of conditions. Moreover, the reactivity of $ZnO/TiO_2/g\text{-}C_3N_4$ NPs happened due to photoinduced electron transfer across NPs, and the weight reduction suggests bond scission with the generation of volatile substances such as H_2O, CO_2, and volatile organic molecules [59–61].

Equation (1) was used to calculate the $ZnO/TiO_2/g\text{-}C_3N_4$/PVC NCs' film degradation efficiency. After 240 hours of solar radiation, the PVC film containing (5:5:2%) $ZnO/TiO_2/g\text{-}C_3N_4$ NPs had a degradation efficiency of 39.16%.

$$\text{Degradation efficiency (\%)} = WL_i - WL_f/WL_i \times 100 \qquad (1)$$

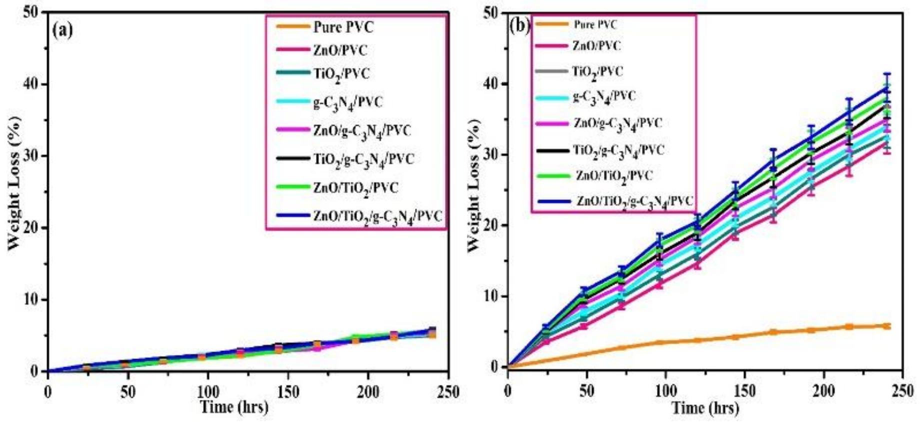

Figure 7. Weight loss (%) of pure PVC films, ZnO/PVC NCs films, TiO_2/PVC NCs films, $g\text{-}C_3N_4/PVC$ NCs films, $ZnO/g\text{-}C_3N_4/PVC$ NCs films, $TiO_2/g\text{-}C_3N_4/PVC$ NCs films, $ZnO/TiO_2/PVC$ NCs films, and $ZnO/TiO_2/g\text{-}C_3N_4/PVC$ NCs films **(a)** under darkness; **(b)** solar light irradiation.

Thus, following a 240-hour exposure period, WL_i represents the initial weight loss of $ZnO/TiO_2/g\text{-}C_3N_4/PVC$ NCs film exposed to solar light, and WL_f represents the final weight loss of $ZnO/TiO_2/g\text{-}C_3N_4/PVC$ NCs film exposed to solar light.

Weight loss analysis (WLA) revealed bond scission and the emission of volatile compounds resulting from the degrading process of $ZnO/TiO_2/g\text{-}C_3N_4/PVC$ NCs film during solar irradiation [62].

The weight loss data is shown against time (h) in Figure 8, and an exponential equation representing first-order kinetics was fitted to the data:

$$dW_t/dt = -kt \qquad (2)$$

Integration of equation (2) gives:

$$\log_{10} W_t = -kt/2{:}303 + \log_{10} W_o \qquad (3)$$

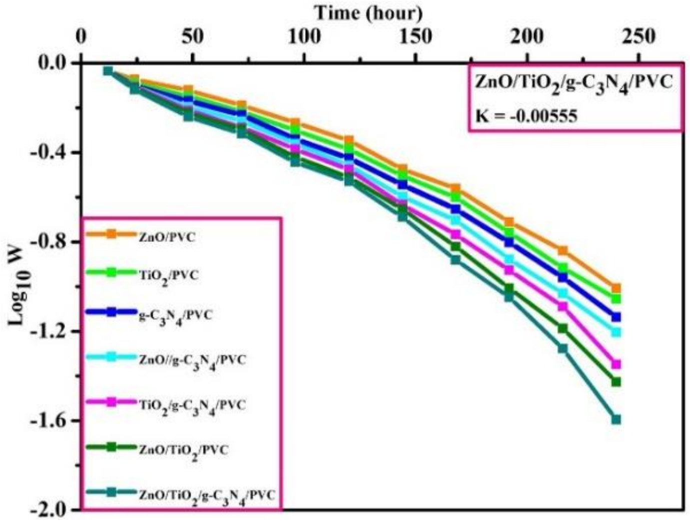

Figure 8. A first-order reaction plotting data on weight reduction against time.

Table 1. The process of photodegradation's kinetic parameters.

S. No	Photocatalyst	W_o (g)	k (h^{-1})	R^2
1	ZnO/PVC	1.0009	3.98×10^{-3}	0.9427
2	TiO_2/PVC	1.0000	4.23×10^{-3}	0.96268
3	$g\text{-}C_3N_4/PVC$	1.0010	3.9×10^{-3}	0.95909
4	$ZnO/gC_3N_4/PVC$	1.0002	3.92×10^{-3}	0.95949
5	$TiO_2/gC_3N_4/PVC$	1.0004	4.12×10^{-3}	0.96184
6	$ZnO/TiO_2/PVC$	1.0007	4.91×10^{-3}	0.96719
7	$ZnO/TiO_2/gC_3N_4/PVC$	1.0014	5.55×10^{-3}	0.97686

The molecular structure of the NC films was observed using FT-IR both before and after 240 hours of irradiation. The amount of oxidation of $ZnO/TiO_2/g\text{-}C_3N_4/PVC$ NCs films, both treated and untreated, has been determined by measuring the absorbance of carbonyl groups (1800–1700 cm^{-1}) in their FT-IR spectrum. Equation (4) was used to calculate the carbonyl index (CI).

$$CI = A_{1800\text{–}1700\ cm^{-1}} / A_{1380\text{–}1375\ cm^{-1}} \quad (4)$$

Where $A_{1800\text{-}1700}\ cm^{-1}$ is the average absorbance of the carbonyl (>C=O) peak at 1800-1700 cm^{-1} and $A_{1380\text{-}1375}\ cm^{-1}$ is the absorbance of the methylene ($-CH_2$) scissoring peak at 1380-1375 cm^{-1} [62].

CI values for $ZnO/TiO_2/g\text{-}C_3N_4/PVC$ NCs MPs films exposed to solar light were 0.16 and 0.12, respectively, for films not exposed to solar light. When compared to the original PVC MPs, the $ZnO/TiO_2/g\text{-}C_3N_4/PVC$ NCs films showed a significant decrease in crystallinity and carbonyl indexes, as much as 2.84% lower. This difference suggests a higher carbonyl (−C=O) breakdown product concentration is produced upon exposure to solar light irradiation. These findings suggest that $ZnO/TiO_2/g\text{-}C_3N_4$ NPs can enhance PVC film degradation when exposed to sun radiation.

Different characteristic bands are CH_2 bend at 1424 cm^{-1}, CH bend at 1328 cm^{-1}, CH bend at 1245 cm^{-1}, C-C stretch at 1093 cm^{-1}, CH_2 rocking at 966 cm^{-1}, and C-Cl stretching at 900–600 cm^{-1}, which suggest the presence of PVC films (Figure 9) [63–65].

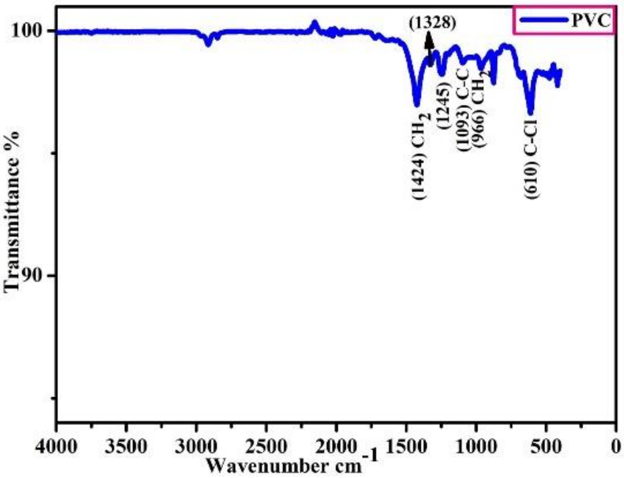

Figure 9. FT-IR spectrum of pure PVC film.

The FT-IR spectrum of ZnO/PVC NCs films, TiO_2/PVC NCs films, $g\text{-}C_3N_4/PVC$ NCs films, $ZnO/g\text{-}C_3N_4/PVC$ NCs films, $TiO_2/g\text{-}C_3N_4/PVC$ NCs films, $ZnO/TiO_2/PVC$ NCs films, and $ZnO/TiO_2/g\text{-}C_3N_4/PVC$ NCs films before sunlight irradiation shows a band at 1725–1705 cm^{-1} assigned to carbonyl (-C=O) groups, the absorption peaks for $g\text{-}C_3N_4$ at 1650–1200 cm^{-1} corresponded to the stretching vibration mode of the C=N bond and the C-N bond in aromatic heterocycles, 1424 cm^{-1} to CH_2 rock, CH bend at 1245 cm^{-1}, 966 cm^{-1} to CH_2 rock, 900–700 cm^{-1} is assigned to TiO_2, 836 cm^{-1} the out-of-plane bending vibration mode of the triazine structure, 900–700 to C-Cl, and 600–400 cm^{-1} to Zn-O stretching vibration (Figure 10a). The bands of ZnO/PVC NCs films, TiO_2/PVC NCs films, $g\text{-}C_3N_4/PVC$ NCs films, $ZnO/g\text{-}C_3N_4/PVC$ NCs films, $TiO_2/g\text{-}C_3N_4/PVC$ NCs films, $ZnO/TiO_2/PVC$ NCs films, and $ZnO/TiO_2/g\text{-}C_3N_4/PVC$ NCs films after sunlight irradiation for 240 h at the band at 1725–1705 cm^{-1} are assigned to C=O bond, the absorption peaks for $g\text{-}C_3N_4$ at 1650–1200 cm^{-1}

corresponded to the stretching vibration mode of the C=N bond and the C-N bond in aromatic heterocycles, 1424 cm^{-1} to CH_2 rock, CH bend at 1245 cm^{-1}, 966 cm^{-1} to CH_2 rock, 900–700 cm^{-1} is assigned to TiO_2, 836 cm^{-1} the out-of-plane bending vibration mode of the triazine structure, 900–600 to C-Cl, and 600–400 cm^{-1} to Zn-O stretching vibration (Figure 10b). For photo-irradiated various films of PVC after sunlight irradiation for 240 h (Figure 10), several new functional peaks appeared in the spectrum. The intensity of carbonyl groups in ZnO/TiO_2/g-C_3N_4/PVC NCs films after sunlight irradiation for 240 h was the strongest among ZnO/PVC NCs films, TiO_2/PVC NCs films, g-C_3N_4/PVC NCs films, ZnO/g-C_3N_4/PVC NCs films, TiO_2/g-C_3N_4/PVC NCs films, and ZnO/TiO_2/PVC NCs films (Figure 10b).

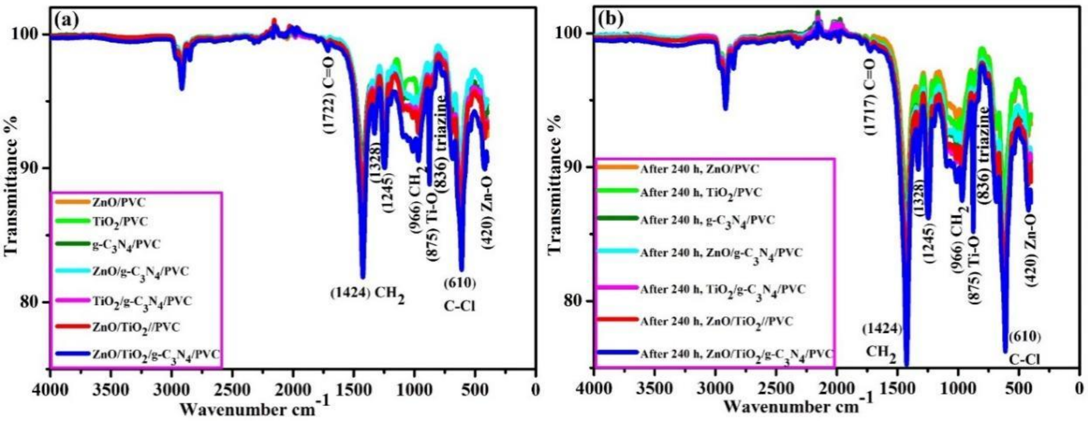

Figure 10. FT-IR spectrum of ZnO/PVC NCs film, TiO_2/PVC NCs film, g-C_3N_4/PVC NCs film, ZnO/g-C_3N_4/PVC NCs film, TiO_2/g-C_3N_4/PVC NCs film, ZnO/TiO_2/PVC NCs film, and ZnO/TiO_2/g-C_3N_4/PVC NCs film **(a)** before 240 h of solar radiation naturally; **(b)** after 240 h of solar irradiation naturally.

3.6.1. Thermal stability of PVC films.

The results of a TGA measurement used to evaluate the ZnO/TiO_2/g-C_3N_4/PVC NCs film's thermal stability and degradation are shown in Figure 11. The film samples of ZnO/TiO_2/g-C_3N_4/PVC NCs that were photo-irradiated and non-irradiated underwent two stages of thermal decomposition over the temperature range, as is evident. Generally, the initial decomposition of these films may be attributed to the primary thermal degradation of an unstable amorphous polymer matrix.

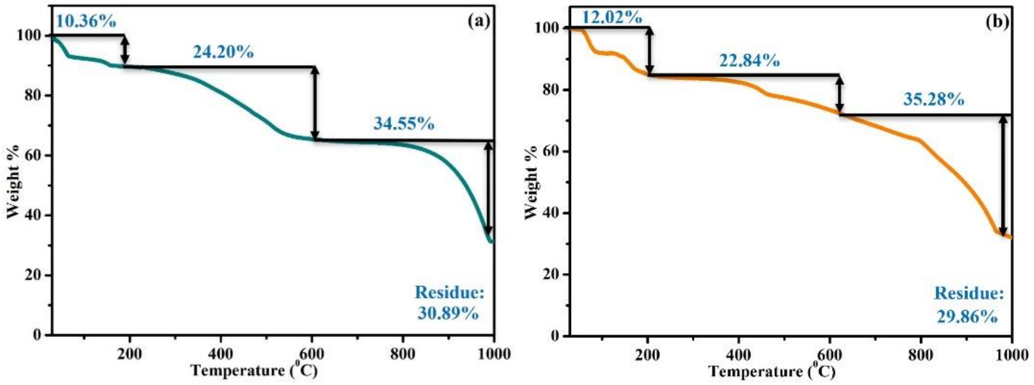

Figure 11. TGA thermograms of ZnO/TiO_2/g-C_3N_4/PVC NCs film **(a)** before 240 h of solar radiation; **(b)** after 240 h of sunlight irradiation.

In contrast, the secondary decomposition may result from the thermal degradation of a compact crystalline PVC film. The thermogram shows that the non-irradiated ZnO/TiO_2/g-C_3N_4/PVC NCs film started to lose weight at 110°C and then drastically degraded up to 600°C, losing 34.56% of its initial weight. In contrast, the photo-irradiated ZnO/TiO_2/g-C_3N_4/PVC

NCs film showed an initial weight loss of 12.02% at 200°C and then further degraded up to 600°C, losing 34.86% of its initial weight. When exposed to 1000°C, the non-irradiated $ZnO/TiO_2/g-C_3N_4/PVC$ NCs film in Figure 11a and the photo-irradiated $ZnO/TiO_2/g-C_3N_4/PVC$ NCs film in Figure 11b both experienced significant degradations, with final weight losses of 68.84% and 70.14%, respectively.

Table 2. Comparison of degradation efficiency (%) of different photocatalysts towards PVC from the literature.

S. No	Plastics	Solvent	Photocatalyst type	Exposure time (h)	Dark (% of degradation	Sunlight (% of degradation	Ref
1	PVC	DMF	$g-C_3N_4$	120 h	-	58%	[32]
2	PVC	-	TiO_2	60 h	-	1.4%	[33]
3	PVC	-	ZnO	3 h	-	12%	[34]
4	PVC	Cyclohexane	ZnO	90 min	-	14.2%	[35]
5	PVC	-	ZnO	7200 sec	-	UV light (20%)	[66]
6	PVC	-	TiO_2/GO	12 h	-	UV light 70.14%	[67]
7	PVC	Cyclohexanone	Fe/ZnO	210 min	-	4.84%	[68]
8	PVC	DMF	ZnO	240 h	5.01 ± 0.06%	31.74 ± 0.10%	This study
9	PVC	DMF	TiO_2	240 h	5.09 ± 0.05%	32.60 ± 0.20%	
10	PVC	DMF	$g-C_3N_4$	240 h	5.21 ± 0.10%	33.96 ± 0.30%	
11	PVC	DMF	$ZnO/g-C_3N_4$	240 h	5.37 ± 0.12%	35.00 ± 0.06%	
12	PVC	DMF	$TiO_2/g-C_3N_4$	240 h	5.56 ± 0.07%	37.02 ± 0.12%	
13	PVC	DMF	ZnO/TiO_2	240 h	5.67 ± 0.08%	38.00 ± 0.14%	
14	PVC	DMF	$ZnO/TiO_2/g-C_3N_4$	240 h	5.78 ± 0.10%	39.86 ± 0.26%	

In summary, Gou *et al.* [32] reported 58% degradation using $g-C_3N_4$/PVC NCs as photocatalysts after 120 h of sunlight exposure in a DMF medium. Xiao-jing *et al.* [33] used TiO_2-PVC NCs for their degradation after 60 h of sunlight exposure and reported 1.4% degradation. A. Roy *et al.* [34] used photocatalyst ZnO NPs and reported 12% degradation of PVC film under sunlight exposure for a period of 3 h. Sil *et al.* [35] used photocatalyst ZnO NPs and reported 14.2% degradation of PVC film under sunlight exposure for a period of 90 min in a cyclohexane medium. Chakrabarti *et al.* [66] observed 20% degradation of PVC in the presence of photocatalyst ZnO under UV exposure of 7200 sec. Hiremath *et al.* [67] reported excellent degradation efficiency of TiO_2/GO photocatalyst (70.14%) on PVC under UV light exposure for 12 h. Das *et al.* [68] found 4.84% degradation of PVC by photocatalyst Fe/ZnO after exposure to sunlight for 210 min in cyclohexane solvent. In this study, we found the degradation of PVC films (39.86 ± 0.26%) after exposure to sunlight for 240 h in DMF medium (Table 2). Specifically, pure PVC film, ZnO/PVC NCs film, TiO_2/PVC NCs film, $g-C_3N_4$/PVC NCs film, $ZnO/g-C_3N_4/PVC$ NCs film, $TiO_2/g-C_3N_4/PVC$ NCs film, $ZnO/TiO_2/PVC$ NCs film, and $ZnO/TiO_2/g-C_3N_4/PVC$ NCs films degrade 5.78 ± 0.10%, 31.74 ± 0.10%, 32.60 ± 0.20%, 33.96 ± 0.30%, 35.00 ± 0.06%, 37.02 ± 0.12%, 38.00 ± 0.14%, and 39.86 ± 0.26%, respectively (Table 2). $ZnO/TiO_2/g-C_3N_4/PVC$ NCs films show high degradation of PVC films (39.86 ± 0.26%) compared to various PVC films.

3.6.2. SEM-EDX morphological features.

We can see the effect of photodegradation on the surface morphology of $ZnO/TiO_2/g-C_3N_4/PVC$ NCs films before and after 240 hours of sun exposure using SEM micrographs (Figure 12). Before 240 hours of solar exposure, the surface of $ZnO/TiO_2/g-C_3N_4/PVC$ NCs films was naturally uniform and smooth, with no significant degradation or morphological impacts on the surface roughness that emerged on ZnO/TiO_2/g-C_3N_4/PVC NCs films surfaces (Figure 12a). The presence of C, N, O, Ti, and Zn elements in the SEM-EDS image of ZnO/TiO_2/g-C_3N_4/PVC NCs films before 240 h of solar radiation (Figure 12c). Degradation activities were seen after 240 hours of natural solar radiation exposure to the ZnO/TiO_2/g-C_3N_4/PVC NCs films. On the surface of the ZnO/TiO_2/g-C_3N_4/PVC NCs films, several spots and cracks formed (Figure 12b). The presence of C, N, O, Ti, and Zn elements in the SEM-EDS image of ZnO/TiO_2/g-C_3N_4/PVC NCs films after 240 h of solar radiation (Figure 12d).

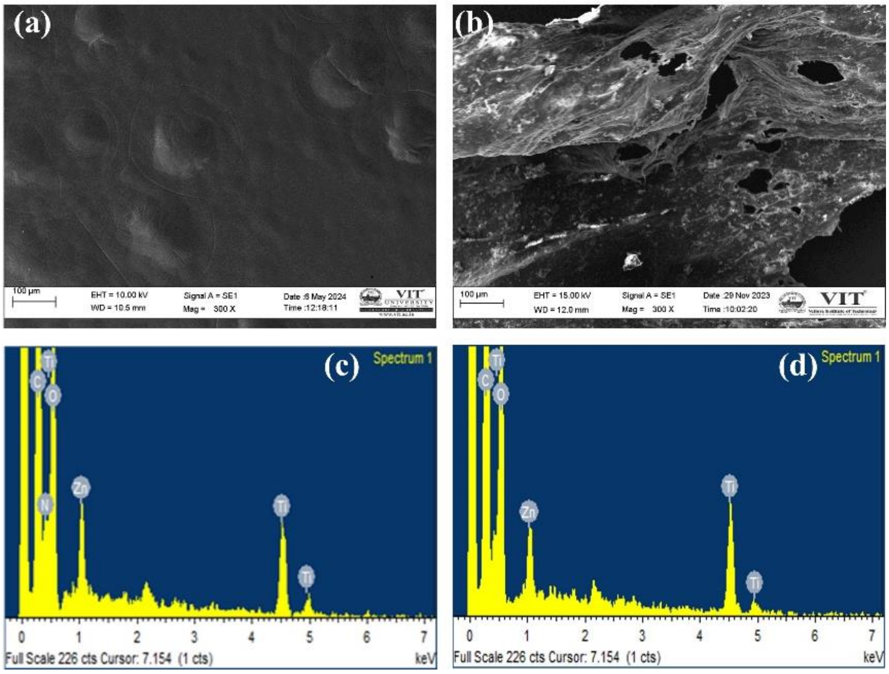

Figure 12. SEM-EDX analysis of ZnO/TiO_2/g-C_3N_4/PVC NCs films **(a, c)** before 240 h of solar radiation; **(b, d)** after 240 h of sunlight irradiation.

3.6.3. Mechanisms for photocatalytic degradation of ZnO/TiO_2/g-C_3N_4/PVC NCs films.

The ZnO/TiO_2/g-C_3N_4/PVC NCs film's photocatalytic degradation is depicted in Figure 13. The band gap of the n-type semiconductor ZnO/TiO_2/g-C_3N_4 is 2.82 eV. When exposed to sufficient light, the ZnO photocatalyst surface produces the photogenerated carriers (h$^+$ and e$^-$). The photogenerated electrons (e$^-$) were created when the electrons that were receiving light energy were energized to move from the valence band (VB) to the conduction band (CB).

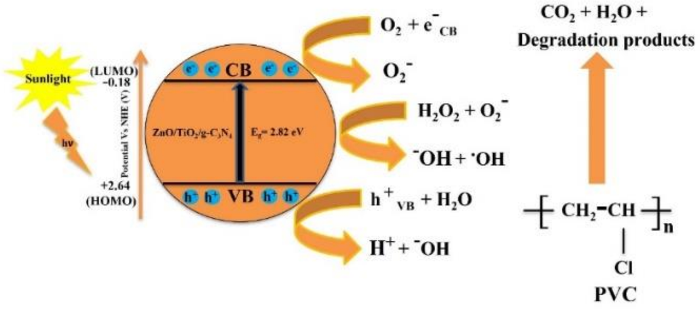

Figure 13. Illustration of the PVC plastic's photodegradation process using the ZnO/TiO_2/g-C_3N_4 photocatalyst.

The photogenerated holes (h$^+$) with oxidant activity were created by the valence band in the meantime (Eqns. 5–6). The separation and migration of ZnO/TiO_2/g-C_3N_4 NPs photogenerated electrons, the prevention of photogenerated carrier conformation, and the photocatalytic effectiveness can all be greatly enhanced by the ability of ZnO/TiO_2/g-C_3N_4 NPs to store and transport electrons (Eqn. 7). Afterwards, O_2 and H_2O adsorbed on the surface of $ZnO/TiO_2/g\text{-}C_3N_4$ form $^{\cdot}O^{2-}$ and ·OH during the photocatalytic process (Eqns. 8–9) [69,70]. A carbon atom-centered free radical chain was created when the $^{\cdot}O^{2-}$ and ·OH attacked the PVC molecular chain. An oxygen-containing group was produced by the interaction with O_2 (Eqns. 10–11), which then followed additional reactions and broke down into smaller molecular compounds (Eqn. 12). Finally, under ideal circumstances, the small-molecule compounds change into CO_2 and H_2O (Eqns. 13–15) [71,72]. The reaction in (Eqns. 5–15) is as follows:

$$ZnO/TiO_2/g\text{-}C_3N_4 + h\nu \rightarrow ZnO/TiO_2/g\text{-}C_3N_4^{*}\,(e^{-} + h^{+}) \tag{5}$$

$$ZnO/TiO_2/g\text{-}C_3N_4\,(h^{+}) + H_2O \rightarrow ZnO/TiO_2/g\text{-}C_3N_4 + {}^{\cdot}OH + H^{+} \tag{6}$$

$$ZnO/TiO_2/g\text{-}C_3N_4^{*}\,(e^{-}) + O_2 \rightarrow ZnO/TiO_2/g\text{-}C_3N_4 + O_2^{\cdot -} \tag{7}$$

$$O_2^{\cdot -} + H^{+} \rightarrow {}^{\cdot}O_2H \tag{8}$$

$${}^{\cdot}O_2H + H_2O \rightarrow {}^{\cdot}OH + H_2O_2 \tag{9}$$

$$\text{-}(CH_2CHCl)\text{-} + {}^{\cdot}OH \rightarrow \text{-}({}^{\cdot}CHCHCl)\text{-} + H_2O \tag{10}$$

$$\text{-}({}^{\cdot}CHCHCl)\text{-} + O_2 \rightarrow \text{-}({}^{\cdot}CH(OO^{\cdot})CHCl)\text{-} \tag{11}$$

$$\text{-}({}^{\cdot}CH(OO^{\cdot})CHCl)\text{-} + \text{-}(CH_2CHCl)\text{-} \rightarrow \text{-}({}^{\cdot}CH(OOH)CHCl)\text{-} + \text{-}({}^{\cdot}CHCHCl)\text{-} \tag{12}$$

$$\text{-}({}^{\cdot}CH(OOH)CHCl)\text{-} + h\nu \rightarrow \text{-}({}^{\cdot}CH({}^{\cdot}O)CHCl)\text{-} + {}^{\cdot}OH \tag{13}$$

$$\text{-}({}^{\cdot}CH({}^{\cdot}O)CHCl)\text{-} + \text{-}(CH_2CHCl)\text{-} \rightarrow \text{-}({}^{\cdot}CH_2(CHCl)CHO)\text{-} + \text{-}{}^{\cdot}CHCl(CH_2CHCl) \tag{14}$$

$$\text{-}{}^{\cdot}CHCl(CH_2CHCl)\text{-} + O_2 \rightarrow CO_2 + H_2O \tag{15}$$

3.6.4. Recyclability and stability study of $ZnO/TiO_2/g\text{-}C_3N_4$ NPs.

The recyclability of $ZnO/TiO_2/g\text{-}C_3N_4$ NPs in PVC film was tested for up to five cycles to ensure their stability. After the first cycle, $ZnO/TiO_2/g\text{-}C_3N_4$/PVC NC films were repeatedly washed with DDW. In a 50-ml vial, $ZnO/TiO_2/g\text{-}C_3N_4$/PVC NCs films were added to 20 ml of DMF. It was ultrasonicated for 10 minutes and centrifuged. Then, a 50 ml vial was placed on a stand for 30 minutes. PVC films in the DMF solvent were filtered out of the vial. The remaining $ZnO/TiO_2/g\text{-}C_3N_4$ NPs settled at the bottom. The $ZnO/TiO_2/g\text{-}C_3N_4$ NPs were repeatedly washed with DDW and centrifuged. It was then allowed to dry overnight at 80°C. The photocatalyst that had been restored was once again used in degradation reactions. The photocatalytic degradation efficiency of $ZnO/TiO_2/g\text{-}C_3N_4$ NPs was reported to be around five cycles. The first cycle had a degradation efficiency of around 87.48%, which was reduced to 78.14% by the fifth cycle (Figure 14a). The stability of $ZnO/TiO_2/g\text{-}C_3N_4$ NPs was determined by comparing the FT-IR and XRD analyses of freshly synthesized and recovered $ZnO/TiO_2/g\text{-}C_3N_4$ NPs following the degrading reactions (Figure 14b and c). The results indicate that there is no noticeable difference between freshly synthesized and recovered catalysts. As a result, $ZnO/TiO_2/g\text{-}C_3N_4$ NPs are extremely stable and can be used as a photocatalyst for PVC MP film degradation.

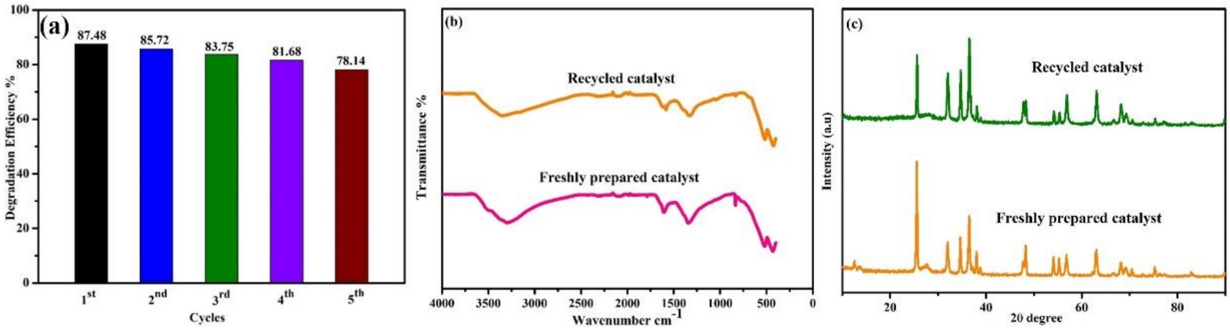

Figure 14. Recyclability of **(a)** $ZnO/TiO_2/g\text{-}C_3N_4$ NPs; **(b)** FT-IR spectrum of $ZnO/TiO_2/g\text{-}C_3N_4$ NPs; **(c)** XRD of $ZnO/TiO_2/g\text{-}C_3N_4$ NPs towards PVC film.

4. Conclusions

This present research provides a different approach for the white synthesis of $ZnO/TiO_2/g\text{-}C_3N_4$ NP photocatalysts. $ZnO/TiO_2/g\text{-}C_3N_4$ NPs exhibit an SPR band at 407 nm, and their ZnO stretching frequencies, which range from 600 to 400 cm^{-1}, are within the metal-oxygen stretching frequencies, which are 900 to 700 cm^{-1}. The $ZnO/TiO_2/g\text{-}C_3N_4$/PVC NCs film's sunlight photocatalytic performance is greater than that of various PVC NCs films, as per weight loss data. The formation of carbonyl groups and the physical degradation of the polymer matrix can assist in the degradation of PVC plastic film. CI values for $ZnO/TiO_2/g\text{-}C_3N_4$/PVC NCs MPs films exposed to solar light were 0.16 and 0.12, respectively, for films not exposed to solar light. When compared to the original PVC MPs, the $ZnO/TiO_2/g\text{-}C_3N_4$/PVC NCs films showed a significant decrease in crystallinity and carbonyl indexes, as much as 2.84% lower. The efficacy of the $ZnO/TiO_2/g\text{-}C_3N_4$ NPs in degrading PVC is validated by photocatalytic degradation studies. Additionally, we have put forth hypothetical equations that explain the PVC degrading process utilizing $ZnO/TiO_2/g\text{-}C_3N_4$ NPs as a photocatalyst. $g\text{-}C_3N_4$ has the potential to enhance ZnO/TiO_2 photogenerated electron separation and migration, inhibit photogenerated carrier conformation, and accelerate PVC photodegradation. It should come as no surprise that photocatalytic technology offers a workable and efficient remedy for "white pollution."

Funding

There is nothing pertinent regarding the authors' non-financial or financial interests.

Acknowledgments

The author, Jameel Mohammed Musthafa, acknowledges the Vellore Institute of Technology, Vellore (632014), Tamil Nadu, India, for providing the platform for this research. Also, the authors acknowledge the help of Sophisticated Instrumental Facilities (SIF) at VIT in carrying out this research.

Conflicts of Interest

There is no conflict of interest, according to the authors.

References

1. Ma, Y.; Liao, S.; Li, Q.; Guan, Q.; Jia, P.; Zhou, Y. Physical and chemical modifications of poly(vinyl chloride) materials to prevent plasticizer migration - Still on the run. *React. Funct. Polym*. **2020**, *147*, 104458, https://doi.org/10.1016/j.reactfunctpolym.2019.104458.
2. Najafi, V.; Abdollahi. H. Internally plasticized PVC by four different green plasticizer compounds. *Eur. Polym. J*. **2020**, *128*, 109620, https://doi.org/10.1016/j.eurpolymj.2020.109620.
3. Salazar Avalos, A.; Hakkarainen, M.; Odelius, K. Superiorly plasticized PVC/PBSA blends through crotonic and acrylic acid functionalization of PVC. *Polymers* **2017**, *9*, 84, https://doi.org/10.3390/polym9030084.
4. Shen, M.; Song, B.; Zeng, G.; Zhang, Y.; Huang, W.; Wen, X.; Tang, W. Are biodegradable plastics a promising solution to solve the global plastic pollution? *Environ. Pollut*. **2020**, *263*, 114469, https://doi.org/10.1016/j.envpol.2020.114469.
5. Zhang, F.; Zhao, Y.; Wang, D.; Yan, M.; Zhang, J.; Zhang, P.; Ding, T.; Chen, L.; Chen, C. Current technologies for plastic waste treatment: A review. *J. Clean. Prod*. **2021**, *282*, 124523, https://doi.org/10.1016/j.jclepro.2020.124523.
6. An, Y.; Hou, J.; Liu, Z.; Peng, B. Enhanced solid-phase photocatalytic degradation of polyethylene by TiO_2-MWCNTs nanocomposites. *Mater. Chem. Phys*. **2014**, *148*, 387–394, https://doi.org/10.1016/j.matchemphys.2014.08.001.
7. Ji, M.; Chen, L.; Que, J.; Zheng, L.; Chen, Z.; Wu, Z. Effects of transition metal oxides on pyrolysis properties of PVC. *Process. Saf. Environ. Prot*. **2020**, *140*, 211–220, https://doi.org/10.1016/j.psep.2020.04.010.
8. Kaczmarek, H.; Bajer, K. Biodegradation of plasticized poly(vinyl chloride) containing cellulose. *J. Polym. Sci. Pt. B: Polym. Phys*. **2007**, *45*, 903–919, https://doi.org/10.1002/polb.21100.
9. Nabi, I.; Bacha, A-U-R.; Ahmad, F.; Zhang, L. Application of titanium dioxide for the photocatalytic degradation of macro- and micro-plastics: A review. *J. Environ. Chem. Eng*. **2021**, *9*, 105964, https://doi.org/10.1016/j.jece.2021.105964.
10. Wang, D.; Zhang, P.; Yan, M.; Jin, L.; Du, X.; Zhang, F.; Wang, Q.; Ni, B.; Chen, C. Degradation mechanism and properties of debris of photocatalytically degradable plastics LDPE-TiO_2 vary with environments. *Polym. Degrad. Stab*. **2022**, *195*, 109806, https://doi.org/10.1016/j.polymdegradstab.2021.109806.
11. Silva, A.B.; Costa, M.F.; Duarte, A.C. Biotechnology advances for dealing with environmental pollution by micro (nano) plastics: lessons on theory and practices. *Curr Opin Environ. Sci. Health*. **2018**, *1*, 30-35, https://doi.org/10.1016/j.coesh.2017.10.005.
12. Asandei, A.D. Polymer synthesis: theory and practice—fundamentals, methods, experiments. D. Braun, H. Cherdron, M. Rehahn, H. Ritter and B. Voit. Springer-Verlag, Berlin, Heidelberg, 2005, 4th edn. ISBN 3-540-20770-8. pp 386, *Polym. Int*. **2005**, *55*, 125-126, https://doi.org/10.1002/pi.1938.
13. Kang, J.; Zhou, L.; Duan, X.; Sun, H.; Ao, Z.; Wang, S. Degradation of cosmetic microplastics via functionalized carbon nanosprings. *Matter* **2019**, *1*, 745-758, https://doi.org/10.1016/j.matt.2019.06.004.
14. Liu, P.; Qian, L.; Wang, H.; Zhan, X.; Lu, K.; Gu, C.; Gao, S. New insights into the aging behavior of microplastics accelerated by advanced oxidation processes. *Environ. Sci. Technol*. **2019**, *53*, 3579-3588, https://doi.org/10.1021/acs.est.9b00493.
15. Ding, W.; Hu, L.; Dai, J.; Tang, X.; Wei, R.; Sheng, Z.; Liang, C.; Shao, D.; song, W.; Liu, Q.; Chen, M.; Zhu, X.; Chou, S.; Zhu, X.; Chen, Q.; Sun, Y.; Xue Dou, S. Highly ambient-stable 1T-MoS_2 and 1T-WS_2 by hydrothermal synthesis under high magnetic fields. *ACS Nano*. **2019**, *13*, 1694-1702, https://doi.org/10.1021/acsnano.8b07744.
16. Basumatary, B.; Basumatary, R.; Ramchiary, A.; Konwar, D. Evaluation of Ag@ TiO_2/WO_3 heterojunction photocatalyst for enhanced photocatalytic activity towards methylene blue degradation. *Chemosphere*. **2022**, *286*, 131848, https://doi.org/10.1016/j.chemosphere.2021.131848.
17. Ibukun, O.; Jeong, H.K. Tailoring titanium dioxide by silver particles for photocatalysis. *Curr.Appl.Phys*. **2020**, *20*, 23-28, https://doi.org/10.1016/j.cap.2019.10.009.
18. Di Paola, A.; García-Lopez, E.; Marcì, G.; Palmisano, L. A survey of photocatalytic materials for environmental remediation. *J. Hazard. Mater*. **2012**, 211-212, 3-29, https://doi.org/10.1016/j.jhazmat.2011.11.050.

19. Das, R.; Sarkar, S.; Kumar, R.; Ramarao, S.D.; Cherevotan, A.; Jasil, M.; Vinod, C.P.; Singh, A.K.; Peter, S.C. Noble-metal-free heterojunction photocatalyst for selective CO_2 reduction to methane upon induced strain relaxation. *ACS Catal*. **2022**, *12*, 687-697, https://doi.org/10.1021/acscatal.1c04587.
20. Chen, J.; Tang, T.; Feng, W.; Liu, X.; Yin, Z.; Zhang, X.; Chen, J.; Cao, S. Large-scale synthesis of p-n heterojunction Bi_2O_3/TiO_2 nanostructures as photocatalysts for removal of antibiotics under visible light. *ACS Applied Nano Materials* **2021**, *5*, 1296-1307, https://doi.org/10.1021/acsanm.1c03851.
21. Li, R.; Zhang, F.; Wang, D.; Yang, J.; Li, M.; Zhu, J.; zhou, X.; Han, H.; Li, C. Spatial separation of photogenerated electrons and holes among {010} and {110} crystal facets of $BiVO_4$. *Nat. Commun*. **2013**, *4*, 1432, https://doi.org/10.1038/ncomms2401.
22. Wang, Q.; Nakabayashi, M.; Hisatomi, T.; Sun, S.; Akiyama, S.; Wang, Z.; Pan, Z.; Xiao, X.; Watanabe, T.; Yamada, T.; Shibata, N.; Takata, T.; Domen, K. Oxysulfide photocatalyst for visible-light-driven overall water splitting. *Nat. Mater*. **2019**, *18*, 827-832, https://doi.org/10.1038/s41563-019-0399-z.
23. Maeda, K.; Sakamoto, N.; Ikeda, T.; Ohtsuka, H.; Xiong, A.; Lu, D.; Kanehara, M.; Teranishi, T.; Domen, K. Preparation of Core-Shell-Structured Nanoparticles (with a Noble-Metal or Metal Oxide Core and a Chromia Shell) and Their Application in Water Splitting by Means of Visible Light. *Chem-A. Eur. J*. **2010**, *16*, 7750-7759, https://doi.org/10.1002/chem.201000616.
24. Srikant, V.; Clarke, D.R. On the optical band gap of zinc oxide. *J. Appl. Phys*. **1998**, *83*, 5447-5451, https://doi.org/10.1063/1.367375.
25. Sakthivel, S.; Neppolian, B.; Shankar, M.V.; Arabindoo, B.; Palanichamy, M.; Murugesan, V. Solar photocatalytic degradation of azo dye: comparison of photocatalytic efficiency of ZnO and TiO_2. *Sol. Energy Mater Sol. Cells* **2003**, *77*, 65-82, https://doi.org/10.1016/S0927-0248(02)00255-6.
26. Fouad, O.A.; Ismail, A.A.; Zaki, Z.I.; Mohamed, R.M. Zinc oxide thin films prepared by thermal evaporation deposition and its photocatalytic activity. *Appl. Catal. B: Environ*. **2006**, *62*, 144-149, https://doi.org/10.1016/j.apcatb.2005.07.006.
27. Khodja, A.A.; Sehili, T.; Pilichowski, J.F.; Boule, P. Photocatalytic degradation of 2-phenylphenol on TiO_2 and ZnO in aqueous suspensions. *J. Photochem. Photobiol. A: Chem*. **2001**, *141*, 231-239, https://doi.org/10.1016/S1010-6030(01)00423-3.
28. Fujishima, A.; Rao, T.N.; Tryk, D.A. Titanium dioxide photocatalysis. *J. Photochem. Photobiol. C: Photochem. Rev*. **2000**, *1*, 1-21, https://doi.org/10.1016/S1389-5567(00)00002-2.
29. Pant, H.R.; Pant, B.; Sharma, R.K.; Amarjargal, A.; Kim, H.J.; Park, C.H.; Tijing, L.D.; Kim, C.S. Antibacterial and photocatalytic properties of $Ag/TiO_2/ZnO$ nano-flowers prepared by facile one-pot hydrothermal process. *Ceram. Int*. **2013**, *39*, 1503-1510, https://doi.org/10.1016/j.ceramint.2012.07.097.
30. Pant, B.; Ojha, G.P.; Kuk, Y.S.; Kwon, O.H.; Park, Y.W.; Park, M. Synthesis and characterization of ZnO-TiO_2/carbon fiber composite with enhanced photocatalytic properties. *Nanomaterials* **2020**, *10*, 1960, https://doi.org/10.3390/nano10101960.
31. Kighuta, K.; Gopalan, A.I.; Lee, D.E.; Saianand, G.; Hou, Y.L.; Park, S.S.; Lee, K.P.; Lee, J.C.; Kim, W.J. Optimization and modeling of efficient photocatalytic TiO_2-ZnO composite preparation parameters by response surface methodology. *J. Environ. Chem. Eng*. **2021**, *9*, 106417, https://doi.org/10.1016/j.jece.2021.106417.
32. Gou, N.; Yang, W.; Gao, S.; Li, Q. Incorporation of Ultrathin Porous Metal-free Graphite Carbon Nitride Nanosheets in Polyvinyl Chloride for Efficient Photodegradation. *J. Hazard. Mater*. **2023**, *447*, 130795, https://doi.org/10.1016/j.jhazmat.2023.130795.
33. Xiao-Jing, L.; Guan-Jun, Q.; Jie-Rong, C. The effect of surface modification by nitrogen plasma on photocatalytic degradation of polyvinyl chloride films. *Appl. Surf. Sci*. **2008**, *254*, 6568-6574, https://doi.org/10.1016/j.apsusc.2008.04.024.
34. Roy, A.; Maitra, S.; Chakrabarti, S. Sonochemical syntheses of iron doped zinc oxide nanoparticles at different sonication powers and temperatures with their application for photocatalytic degradation of PVC-ZnO composite film. *Int. J. Nanoparticles* **2018**, *10*, 178-195, https://doi.org/10.1504/IJNP.2018.094040.
35. Sil, D.; Chakrabarti, S. Photocatalytic degradation of PVC-ZnO composite film under tropical sunlight and artificial UV radiation: A comparative study. *Sol. Energy*. **2010**, *84*, 476-485, https://doi.org/10.1016/j.solener.2009.09.012.
36. Wang, P.; Yap, P.S.; Lim, T.T. C-N-S tridoped TiO_2 for photocatalytic degradation of tetracycline under visible-light irradiation. *Appl. Catal. A: Gen*. **2011**, *399*, 252-261, https://doi.org/10.1016/j.apcata.2011.04.008.

37. Bharathi, D.; Ranjithkumar, R.; Chandarshekar, B.; Bhuvaneshwari, V. Preparation of chitosan coated zinc oxide nanocomposite for enhanced antibacterial and photocatalytic activity: as a bionanocomposite. *Int. J. Biol. Macromol*. **2019**, *129*, 989-996, https://doi.org/10.1016/j.ijbiomac.2019.02.061.
38. Tian, J.; Chen, L.; Yin, Y.; Wang, X.; Dai, J.; Zhu, Z.; Liu, X.; Wu, P. Photocatalyst of TiO_2/ZnO nano composite film: preparation, characterization, and photodegradation activity of methyl orange. *Surf. Coat. Technol*. **2009**, *204*, 205-214, https://doi.org/10.1016/j.surfcoat.2009.07.008.
39. Prasannalakshmi, P.; Shanmugam, N. Fabrication of TiO_2/ZnO nanocomposites for solar energy driven photocatalysis. *Mater. Sci. Semicond. Process*. **2017**, *61*, 114-124, https://doi.org/10.1016/j.mssp.2017.01.008.
40. Wang, B.; He, H.; Hao, H.; Li, P.; Cai, H.; Shang, F.; An, B.; Li, X.; Yang, S. Melamine-phytic acid derived supramolecular synthesis of g-C_3N_4 for enhanced solar hydrogen evolution. *Int. J. Hydrog. Energy* **2023**, *48*, 13097-13108, https://doi.org/10.1016/j.ijhydene.2022.12.246.
41. Verma, R.; Singh, S.; Dalai, M.K.; Saravanan, M.; Agrawal, V.V.; Srivastava, A.K. Photocatalytic degradation of polypropylene film using TiO_2 -based nanomaterials under solar irradiation. *Mater. Des*. **2017**, *133*, 10-18, http://dx.doi.org/10.1016/j.matdes.2017.07.042.
42. Zhang, Y.; Sun, T.; Zhang, D. ; Shi, Z.; Zhang, X.; Li, C. Wang, L.; Song, J.; Lin, Q. Enhanced photodegradability of PVC plastics film by codoping nano-graphite and TiO_2. *Polym. Degrad. Stab*. **2020**, *181*, 109332, https://doi.org/10.1016/j.polymdegradstab.2020.109332.
43. Dehury, T.; Rath, C.; Panigrahi, S. Ammonia Sensing Behavior of Green Synthesized ZnO Nanoparticles using Optical Density as Sensing Parameter. *IEEE Sensors Journal*. **2024**, *24*, 13104-13112, https://doi.org/10.1109/JSEN.2023.3318517.
44. Palangi, V.; Macit, M.; Nadaroglu, H.; Taghizadeh, A. Effects of green-synthesized CuO and ZnO nanoparticles on ruminal mitigation of methane emission to the enhancement of the cleaner environment. *Biomass Conv. Bioref*. **2024**, *14*, 5447-5455, https://doi.org/10.1007/s13399-022-02775-9.
45. Halim, W.; Eddahbi, A.; Mouna, S.I.; Kassiba, A.; Ouaskit, S. Synthesis of perfect TiO_2 nanospheres decorated by silver shell nanoparticles for photocatalytic applications. *J. Clust. Sci*. **2024**, *35*, 1777-1786, https://doi.org/10.1007/s10876-024-02614-z.
46. Li, J.; Li, J.; Ma, N.; Guan, L.; Tan, C.; Xia, Z.; Xu, J.; Zuo, J. Preparation of ZnO/TiO_2 NTs-loaded materials and their photocatalytic performance. *Chemical Physics Letters* **2024**, *838*, 141084, https://doi.org/10.1016/j.cplett.2024.141084.
47. Kumar, S.R.A.; Mary, D.V.; Suganya Josephine, G.A.; Sivasamy, A. Hydrothermally synthesized WO_3:CeO_2 supported gC_3N_4 nanolayers for rapid photocatalytic degradation of azo dye under natural sunlight. *Inorganic Chemistry Communications* **2024**, *164*, 112366, https://doi.org/10.1016/j.inoche.2024.112366.
48. Sadek, O.; Touhtouh, S.; Rkhis, M.; Hajjaji, A. Study of the hydroxylation of the TiO_2 thin layer prepared by spin-coating method using FTIR analysis and DFT theory. *Inorganic Chemistry Communications* **2024**, *161*, 112092, https://doi.org/10.1016/j.inoche.2024.112092.
49. Giang, N.T.H.; Huong, L.M.; Hai, N.D.; Quang, D.M.; Thi, D.N.; Quyen, V.P.T.T.; Phong, M.T.; Hieu, N.H. Application of TiO_2/gC_3N_4 for the efficient photosynthesis of hydrogen peroxide. *Diamond and Related Materials* **2023**, *140*, 110506, https://doi.org/10.1016/j.diamond.2023.110506.
50. Andrade-Guel, M.; Cabello-Alvarado, C.; Bartolo-Pérez, P.; Medellin-Banda, D.I.; Ávila-Orta, C.A.; Cruz-Ortiz, B.; Espinosa-Munoz, A.; Cadenas Pliego, G. Surface modification of TiO_2/ZnO nanoparticles by organic acids with enhanced methylene blue and rhodamine B dye adsorption properties. *RSC advances* **2022**, *12*, 28494-28504, https://doi.org/10.1039/D2RA04961A.
51. Nadeem, M.S.; Munawar, T.; Alam, M.M.; Mukhtar, F.; Mahmood, K.; Al-Sehemi, A.G.; Iqbal, F. Effect of Co/Nd co-doping on the structural, optical, and morphological properties of ZnO nanorods grown on silicon substrate Si (100) by hydrothermal method. *Journal of Luminescence*. **2024**, *269*, 120484, https://doi.org/10.1016/j.jlumin.2024.120484.
52. Mondal, S.; Jamal, M.; Ayon, S.A.; Anik, M.J.F.; Billah, M.M. Synergistic enhancement of photocatalytic and antimicrobial efficacy of nitrogen and erbium co-doped ZnO nanoparticles. *Journal of Rare Earths*. **2023**, *42*, 859-868, https://doi.org/10.1016/j.jre.2023.10.002.
53. Wang, X.; Wu, M.; Cui, B.; Li, Y.; Wu, Y.; Wen, Y.; Liu, J.; Li, X.; Ye, S.; Ren, P.; Ji, Z.; Lu, H.; Zhang, D.W.; Wang, R.; Huang, R. Oxygen Vacancy Modulation with TiO_2 Stack Interface Engineering for Ferroelectric $Hf_{0.5}Zr_{0.5}O_2$ Thin Films. *IEEE Electron Device Letters*. **2023**, *45*, https://doi.org/10.1109/LED.2023.3330784.

54. Wang, J.; Peng, Y.; Wang, L.; Yang, X.; Gao, Y. ; Li, X.; Lu, W. Modification of TiO_2 with sodium borohydride and its influence on photovoltaic cell performance. *Ionics* **2024**, *30*, 4271-4279, https://doi.org/10.1007/s11581-024-05551-z.
55. Buu, T.T.; Cong, C.Q.; Quan, V.M.; Ngoc, B.K.; Nam, N.T.H.; Thao, L.T.P.; Tam, D.H.M.; Han, L.G.; Hieu, N.H. Construction of Z-scheme heterojunction TiO_2-ZnO@ Oxygen-doped gC_3N_4 composite for enhancing H_2O_2 photoproduction and removal of pharmaceutical pollutants under visible light. *Surfaces and Interfaces*. **2023**, *43*, 103516, https://doi.org/10.1016/j.surfin.2023.103516.
56. Singh, J.; Rathi, A.; Rawat, M.; Kumar, V.; Kim, K.H. The effect of manganese doping on structural, optical, and photocatalytic activity of zinc oxide nanoparticles. *Compos. B: Eng*. **2019**, *166*, 361-370, https://doi.org/10.1016/j.compositesb.2018.12.006.
57. Zhang, J.; Kuang, M.; Cao, Y.; Ji, Z. Environment-friendly ternary $ZnO/ZnFe_2O_4/TiO_2$ composite photocatalyst with synergistic enhanced photocatalytic activity under visible-light irradiation. *Solid State Sci*. **2022**, *129*, 106913, https://doi.org/10.1016/j.solidstatesciences.2022.106913.
58. Akhter, P.; Nawaz, S.; Shafiq, I.; Nazir, A.; Shafique, S.; Jamil, F.; Park, Y.K.; Hussain, M. Efficient visible light assisted photocatalysis using ZnO/TiO_2 nanocomposites. *J. Mol. Catal*. **2023**, *535*, 112896, https://doi.org/10.1016/j.mcat.2022.112896.
59. Lankone, R.S.; Wang, J.; Ranville, J.F.; Fairbrother, D.H. Photodegradation of polymer-CNT nanocomposites: effect of CNT loading and CNT release characteristics. *Environ. Sci.: Nano*. **2017**, *4*, 967-982, https://doi.org/10.1039/C6EN00669H.
60. Liang, W.; Luo, Y.; Song, S.; Dong, X.; Yu, X. High photocatalytic degradation activity of polyethylene containing polyacrylamide grafted TiO_2. *Polym. Degrad. Stab*. **2013**, *98*, 1754-1761, https://doi.org/10.1016/j.polymdegradstab.2013.05.027.
61. Thomas, R.T.; Sandhyarani, N. Enhancement in the photocatalytic degradation of low density polyethylene–TiO_2 nanocomposite films under solar irradiation. *RSC Advances* **2013**, *3*, 14080-14087, https://doi.org/10.1039/C3RA42226G.
62. Olajire, A.A.; Mohammed, A.A. Bio-directed synthesis of gold nanoparticles using Ananas comosus aqueous leaf extract and their photocatalytic activity for LDPE degradation. *Adv. Powder Technol*. **2021**, *32*, 600-610, https://doi.org/10.1016/j.apt.2021.01.009.
63. Noda, I.; Dowrey, A.E.; Haynes, J.L.; Marcott, C. Group Frequency Assignments for Major Infrared Bands Observed in Common Synthetic Polymers. In Physical Properties of Polymers Handbook, Mark, J.E., Ed.; Springer New York: New York, NY, **2007**; pp. 395-406, https://doi.org/10.1007/978-0-387-69002-5_22.
64. Beltran, M.; Marcilla, A. Fourier transform infrared spectroscopy applied to the study of PVC decomposition. *Eur. Polym. J*. **1997**, *33*, 1135–1142, https://doi.org/10.1016/S0014-3057(97)00001-3.
65. Malimabe, M.A.; Dejene, B.F.; Swart, H.C.; Motloung, S.V.; Motaung, T.E.; Koao, L.F. Characterization of the incorporated ZnO doped and co-doped with Ce^{3+} and Eu^{3+} nanophosphor powders into PVC polymer matrix. *J. Mol. Struct*. **2020**, *1202*, 127339, https://doi.org/10.1016/j.molstruc.2019.127339.
66. Chakrabarti, S.; Dutta, B.K. Dye-sensitised photocatalytic degradation of PVC-ZnO composite film. Int. *J. Environ. Technol. Manag*. **2008**, *9*, 34-46, https://doi.org/10.1504/IJETM.2008.017858.
67. Hiremath, B.R.; Muttinamath, A. Photocatalytic Degradation of Polyvinyl Chloride Plastic Film by Codoping Graphene Oxide and Titanium Dioxide. *i-Manager's Journal on Civil Engineering*. **2022**, *12*, 1-10, https://doi.org/10.26634/jce.12.3.18975.
68. Das, P.; Roy, A.; Chakrabarti, S. Photocatalytic degradation of the nanocomposite film comprising polyvinyl chloride (PVC) and sonochemically synthesized iron-doped zinc oxide: A comparative study of performances between sunlight and UV radiation. *J. Polym. Environ*. **2017**, *25*, 1231-1241, https://doi.org/10.1007/s10924-016-0894-0.
69. Linsebigler, A.L.; Lu, G.; Yates Jr, J.T. Photocatalysis on TiO_2 surfaces: principles, mechanisms, and selected results. *Chem. Rev*. **1995**, *95*, 735–758, https://doi.org/10.1021/cr00035a013.
70. Zan, L.; Fa, W.; Wang, S. Novel photodegradable low-density polyethylene−TiO_2 nanocomposite film. *Environ. Sci. Technol*. **2006**, *40*, 1681–1685, https://doi.org/10.1021/es051173x.
71. Yousif, E.; Al-Amiery, A.A.; Kadihum, A.; Kadhum, A.A.H.; Mohamad, A.B. Photostabilizing efficiency of PVC in the presence of schiff bases as photostabilizers. *Molecules* **2015**, *20*, 19886–19899, https://doi.org/10.3390/molecules201119665.
72. Cho, S.; Choi, W. Solid-phase photocatalytic degradation of PVC–TiO_2 polymer composites. *J. Photochem. Photobiol. A: Chem*. **2001**, *143*, 221–228, https://doi.org/10.1016/S1010-6030(01)00499-3.